UNIVERSITY *of* York

This is a repository copy of *Capacitively coupled hydrogen plasmas sustained by tailored voltage waveforms::excitation dynamics and ion flux asymmetry*.

White Rose Research Online URL for this paper:
https://eprints.whiterose.ac.uk/103144/

Version: Published Version

White Rose
university consortium
Universities of Leeds, Sheffield & York

eprints@whiterose.ac.uk
https://eprints.whiterose.ac.uk/

Capacitively coupled hydrogen plasmas sustained by tailored voltage waveforms: excitation dynamics and ion flux asymmetry

B Bruneau[1], P Diomede[2,3], D J Economou[2], S Longo[4], T Gans[5], D O'Connell[5], A Greb[5], E Johnson[1] and J-P Booth[6]

[1] LPICM-CNRS, Ecole Polytechnique, Palaiseau 91128, France
[2] Plasma Processing Laboratory, Department of Chemical & Biomolecular Engineering, University of Houston, Houston, TX 77204-4004, USA
[3] FOM Institute DIFFER—Dutch Institute for Fundamental Energy Research, PO Box 6336, Eindhoven 5600 HH, The Netherlands
[4] Dipartimento di Chimica, Universita' degli Studi di Bari, via Orabona 4, Bari 70126, Italy
[5] York Plasma Institute, Department of Physics, University of York, Heslington, York, YO10 5DD, UK
[6] LPP, Ecole Polytechnique-CNRS-Univ Paris-Sud-UPMC, Palaiseau 91128, France

E-mail: bastien.bruneau@polytechnique.edu

CrossMark

Abstract

Parallel plate capacitively coupled plasmas in hydrogen at relatively high pressure (~1 Torr) are excited with tailored voltage waveforms containing up to five frequencies. Predictions of a hybrid model combining a particle-in-cell simulation with Monte Carlo collisions and a fluid model are compared to phase resolved optical emission spectroscopy measurements, yielding information on the dynamics of the excitation rate in these discharges. When the discharge is excited with amplitude asymmetric waveforms, the discharge becomes electrically asymmetric, with different ion energies at each of the two electrodes. Unexpectedly, large differences in the H_2^+ fluxes to each of the two electrodes are caused by the different H_3^+ energies. When the discharge is excited with slope asymmetric waveforms, only weak electrical asymmetry of the discharge is observed. In this case, electron power absorption due to fast sheath expansion at one electrode is balanced by electron power absorption at the opposite electrode due to a strong electric field reversal.

Keywords: tailored voltage waveforms, electrical asymmetry effect, capacitively coupled plasmas, hydrogen discharge, discharge asymmetry, PIC simulations, PROES

(Some figures may appear in colour only in the online journal)

Introduction

Parallel plate capacitively coupled radio-frequency (CCRF) plasmas are commonly used for materials processing applications such as the deposition and etching of thin films. Especially for deposition applications, large area reactors

are generally used, and only minimal geometrical asymmetry is present. When single-frequency (sinusoidal) excitation is used, the energy distribution of ions arriving at the reactor surfaces can then only be controlled by the RF power or the pressure, and will be identical on both electrodes (or electrode and substrate). However, the RF power also determines the deposition rate, and therefore cannot be used to independently vary the ion energy. Furthermore, changing the pressure will lead to significant changes in the deposition chemistry, and may cause the appearance of nanoparticles and
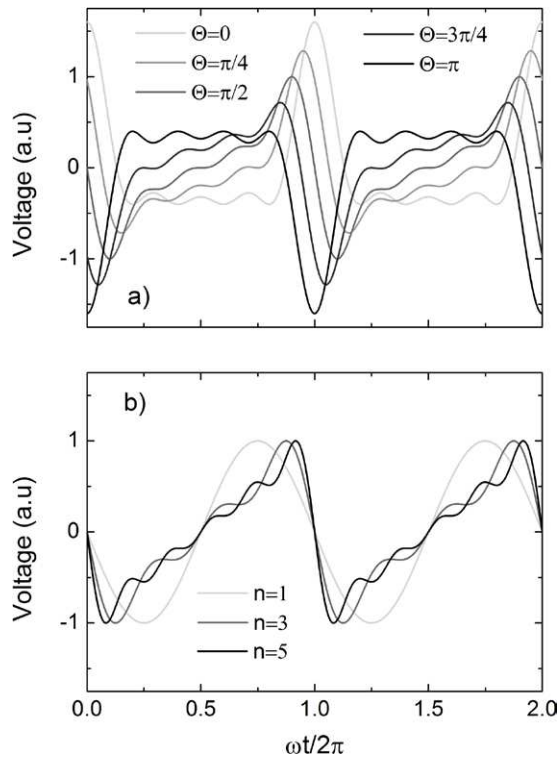
Figure 1. (a) Waveforms according to equation (3) with different phase shifts Θ, for $n = 4$, (b) waveforms according to equation (4), corresponding to sawtooth-up waveforms, with different n, V_0 is chosen to keep V_{PP} equal to two.

powders in the plasma. However, with the use of plasma excitation by voltage waveforms comprising multiple frequencies, it is possible to control the ion energy, for example via the electrical asymmetry effect (EAE), independently of other plasma parameters [1–13] and in particular independently of the ion flux. According to an analytical model developed by Czarnetzki *et al* the self-bias, η [1–3], caused by the EAE can be expressed as:

$$\eta = -\frac{\widetilde{V}_{m1} + \varepsilon \widetilde{V}_{m2}}{1 + \varepsilon} \qquad (1)$$

where $\widetilde{V}_{m1}$ and $\widetilde{V}_{m2}$ are the maximum and the minimum (relative to the temporal average) of the applied voltage waveform $V_{AC}(t)$, respectively, and the symmetry parameter, ε, is defined by:

$$\varepsilon = \left| \frac{\widehat{V}_{sg}}{\widehat{V}_{sp}} \right| \approx \left(\frac{A_p}{A_g} \right)^2 \frac{\bar{n}_{sp}}{\bar{n}_{sg}} \qquad (2)$$

where $\widehat{V}_{sp}$ and $\widehat{V}_{sg}$ are the maximum voltages across the sheaths at the powered and grounded electrodes, respectively, A_p and A_g are the areas of the powered and the grounded electrodes, and $\bar{n}_{sp}$ and $\bar{n}_{sg}$ are the respective mean ion densities in the sheaths. Whereas the EAE was originally proposed for waveforms comprising only two harmonics, the pioneering work on ion energy control using multiple-harmonic waveforms of Wendt *et al* [14, 15] inspired the use of more complex Tailored Voltage Waveforms (TVWs) for plasma excitation to further

enhance the EAE [16]. Such waveforms can be described by the following expression [17]

$$V_{AC}(t) = V_0 \sum_{k=1}^{n} \frac{n - k + 1}{n} \cos(k\omega t + \Theta) \qquad (3)$$

where V_0 is a voltage amplitude factor, n is the number of harmonics, (varied between one and five in this work), ω is the angular frequency, here corresponding to a frequency f of 5 MHz ($\omega = 2\pi f$), and Θ is a phase shift. V_0 is set to give the desired peak-to-peak voltage, V_{PP}. TVWs therefore contain multiple harmonics of the same fundamental frequency f. The phase shift Θ can be varied to control the amplitude asymmetry from a maximum ($\Theta = 0$), to a minimum ($\Theta = \pi$). Such waveforms, with $n = 4$, are shown in figure 1(a) for different values of Θ. The harmonics' amplitudes are chosen to maximize the amplitude asymmetry of the waveform ($\widetilde{V}_{m1}/\widetilde{V}_{m2}$) for $\Theta = 0$ or π (when the waveforms are temporally symmetric) and therefore maximize the accessible range of DC self-bias according to equation (1). For other values of the phase shift the amplitude asymmetry is lower (and is non-existent for $\Theta = \pi/2$), but the waveforms have temporal asymmetry, with differing rise and fall rates.

The use of waveforms that do not exhibit temporal symmetry can produce unexpected dynamics in the plasma, as was recently shown for argon discharges [18–20]. Choosing the harmonics' amplitudes to maximize this second type of waveform asymmetry as follows:

$$V_{AC}(t) = \pm V_0 \sum_{k=1}^{n} \frac{1}{k} \sin(k\omega t) \qquad (4)$$

produces waveforms that are approximations of sawtooths. The minus sign in equation (4) corresponds to sawtooth-up waveforms, while the plus sign corresponds to sawtooth-down waveforms. Such waveforms have slope asymmetry, increasing with the number of harmonics, n, but no amplitude asymmetry. The $1/k$ prefactors maximize the slope asymmetry for a given n. Such sawtooth-up waveforms with different values of n are shown in figure 1(b). Sawtooth waveforms cause fast sheath expansion and slow sheath contraction in front of one electrode, and slow sheath expansion and fast sheath contraction in front of the opposite electrode [20]. As a consequence, a strong asymmetry of the ionization occurs in argon discharges, with larger ionization at the side where the sheath expands rapidly. In relatively high pressure argon discharges a DC self-bias was also shown to appear, despite the absence of amplitude asymmetry ($\widetilde{V}_{m1} = -\widetilde{V}_{m2}$), and was attributed to different mean ion densities in the sheaths ($\varepsilon \neq 1$ in equation (1)), leading to different ion fluxes at each of the electrodes.

More recently, Bruneau *et al* [21] have studied the impact of waveforms with continuously changing amplitude and slope asymmetry, obtained by slightly shifting the higher frequencies from the harmonics. These waveforms are shown to control the shape of the ion flux distribution function, and in particular its width, while keeping the ion flux and mean ion energy constant. They are, however, not used in the present study.
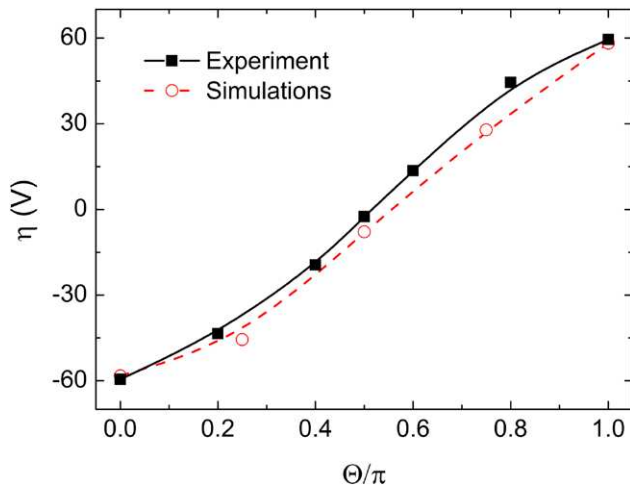
Figure 2. DC self-bias η as a function of the phase shift Θ; the red dashed line and circles represent the results of PIC simulations, while the black solid line and squares represent the experimental data. Lines are a guide to the eye.

Amplitude-asymmetric waveforms (defined by equation (3) with $\Theta = 0$ or π) have been used to grow silicon thin films by PECVD [16, 22–25] including their application to solar cells [26–28]. Most of these studies used the standard discharge chemistry of silane highly diluted in hydrogen, with gas pressures in the Torr range. However, plasma studies of hydrogen discharges excited with TVWs are rather scarce [29–32]. There is hence a need to further study the impact of TVWs on hydrogen discharges under conditions relevant to those used in thin film deposition. In particular, attention should be paid to the spatiotemporal dynamics and not only the time-averaged values of the quantities of interest, since TVWs significantly alter the sheath motion within the RF cycle.

In the present work numerical simulations were carried out using a code developed by the Bari University group. This hybrid code was described in detail in [29, 33]. It self-consistently couples a PIC/MCC description for five charged species (H^+, H_2^+, H_3^+, H^- and electrons) with a reaction-diffusion fluid model for neutrals (15 vibrational levels of the electronic ground state of H_2, and H atoms). The equations of motion for the charged particles are integrated by using the leap-frog method and the electric field is calculated by solving the Poisson equation, with the space charge obtained from a first-order particle-grid interpolation. The field solver and the particle/Monte Carlo solver are coupled by matching the fixed PIC time step Δt with the values of the times between collisions using the modified time step approach [34, 35]. The predictions of this code were recently compared to experimental results in the case of TVWs [29], using $\Theta = 0$ or π in equation (3), with n being varied from 1–3. The simulated ion flux distribution functions (IFDFs) were shown to be in good agreement with those measured experimentally with a quadrupole mass spectrometer (QMS) coupled with an ion energy analyser.

In the present work, the predictions of this hybrid simulation are compared to phase resolved optical emission spectroscopy (PROES) measurements. The experimental setup was presented in [20]. A reactor with an inter-electrode gap of 2.5 cm

was made geometrically symmetric by adding a thick Teflon ring (inner diameter 10 cm), fitted with a $2.5 \times 2.5 \times 10$ cm window of borosilicate glass to allow optical access. The window is placed so that its edges are aligned with the two electrodes. A working pressure of 900 mTorr was used in all experiments, as measured outside the plasma chamber, and the gas flow was kept low to avoid over-pressure inside. The voltage waveform was generated using a computer-controlled arbitrary function generator (AFG) and wideband power amplifier as described previously [16]. The actual waveform at the electrode was monitored by a high voltage probe, and was corrected for distortion using a feedback loop as proposed by Patterson *et al* [15]. An intensified CCD camera (Andor iStar) was synchronized to the AFG, and the phase varied using a delay generator. The intensifier gate of the ICCD camera was 2 ns, therefore giving 100 images within one RF-cycle for a fundamental frequency of 5 MHz. The excitation rate at each position and phase was deconvoluted from the measured H_α emission at 656 nm, using the method proposed in [36], and was compared to the $H(n = 3)$ excitation rate given by the simulations. Although two different processes are compared, these processes have similar energy thresholds and will therefore probe in a comparable way the high energy electron population. This strategy therefore limits us to a qualitative comparison of the dynamics of energetic electrons.

In the following, first the effect of amplitude-asymmetric waveforms (defined by equation (3)) on hydrogen discharges is investigated, and then we focus on the effect of slope-asymmetric waveforms (defined by equation (4)). In both cases the simulated excitation rates and the DC self-bias are compared to experiments. Furthermore the simulations are used to investigate the effect of TVWs on the ion flux and ion flux distribution function (IFDF) at each electrode.

Results

Amplitude asymmetry

In the following section, waveforms according to equation (3) are used, with $n = 4$, i.e. corresponding to the waveforms shown in figure 1(a). The phase shift Θ is varied from 0 to π in order to vary the amplitude asymmetry of the waveform. The neutral gas pressure is kept constant at 900 mTorr, and V_0 is kept constant at 112 V (giving a peak-to-peak voltage $V_{PP} = 350$ V for $\Theta = 0$).

As a first comparison between the experiments and the simulations, figure 2 shows the DC self-bias η, experimentally measured (black solid line and squares) and obtained from simulations (red dashed line and circles) for a phase shift Θ varying from 0 to π. The experimental values have been shifted by $+6$ V (mean value of the DC self-biases measured for $\Theta = 0$ and $\Theta = \pi$) to correct for a small remaining geometrical asymmetry. The agreement between the simulations and experiments is excellent for all values of Θ. The increase of the DC self-bias with Θ is almost linear, as can be expected from equation (1) and from the variation of $\widetilde{V}_{m1}$ and $\widetilde{V}_{m2}$ with Θ in equation (3).
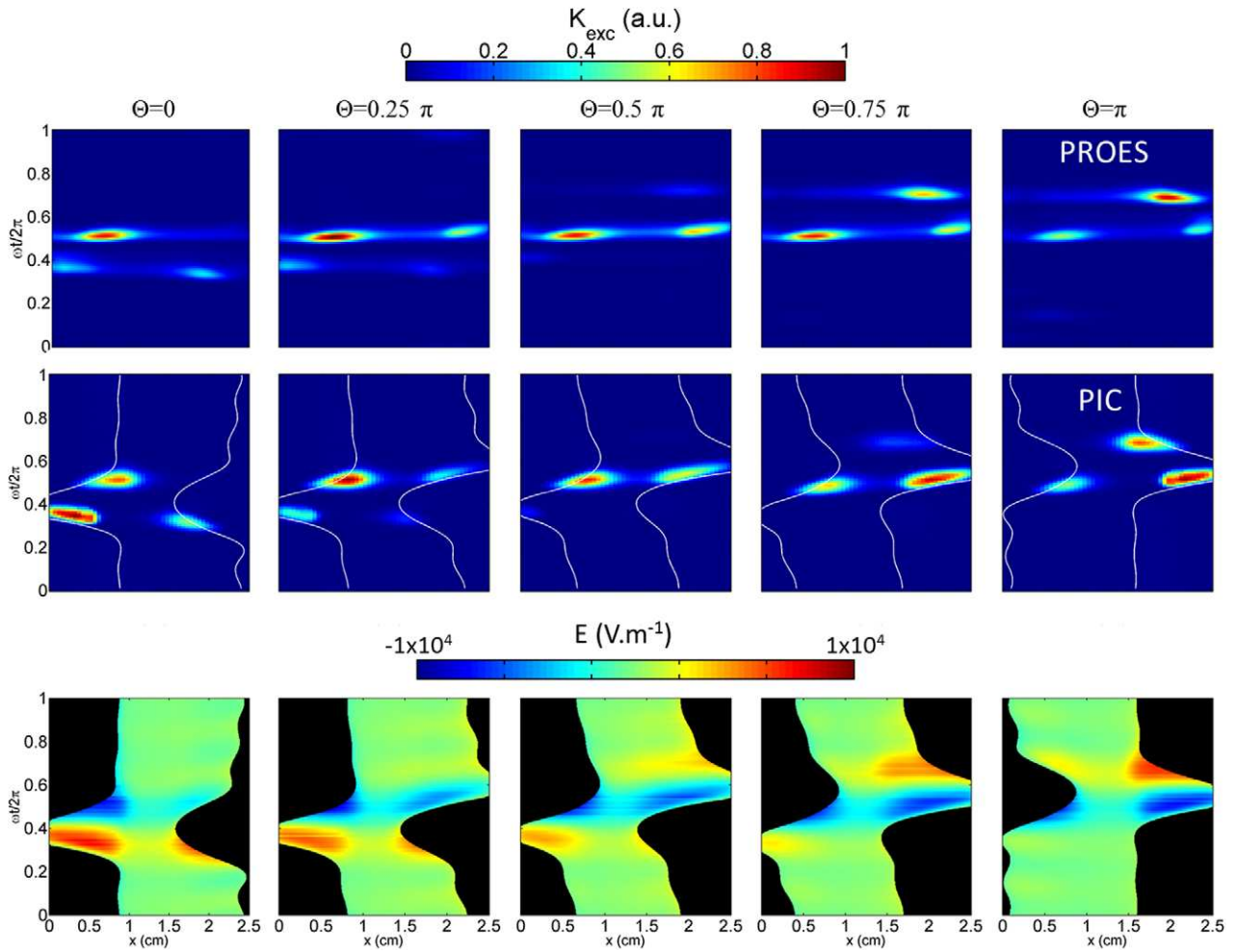
Figure 3. Spatio-temporal excitation rates derived from measurement of the emission line at 656 nm using PROES (top row), and from PIC simulations (middle row), and predicted bulk electric field (bottom row) using waveforms with $n = 4$ frequencies, for different Θ from 0 (left) to π (right); the excitation rates are normalized to the global maximum of the case $\Theta = 0$.

Figure 3 shows the $H(n = 3)$ excitation rate obtained from the optical emission of the H_α line at 656 nm (top row), and the simulated excitation rate (middle row) for different phase shifts Θ. The x-axis represents position (with the powered electrode at $x = 0$ cm and the grounded electrode at $x = 2.5$ cm), while the y-axis represents time and spans one fundamental RF cycle. For both the experiments and the simulations, all images are normalized to the maximum intensity observed for the $\Theta = 0$ case. The sheath edge position, as determined by the Brinkmann criterion [37], is shown as a white line. Also shown is the dynamics of the electric field outside of the sheath regions (the latter areas being shown in black) obtained from the simulations (bottom row). As one can see by comparing the two first rows of the figures, the general excitation features observed in the experiment are qualitatively well reproduced by the simulations. However, the relative amplitudes of individual excitation features differ slightly between the experiments and the simulations. In particular, excitation rates occurring during fast sheath collapses are generally overestimated by the simulations.

Focusing first on the $\Theta = 0$ case and starting at the beginning of the RF cycle, a first excitation peak appears when the

sheath close to the grounded electrode expands. This excitation is due to electron power absorption by sheath expansion, which can be described by the hard-wall model introduced by Godyak [38, 39]. Almost simultaneously, another peak appears close to the powered electrode as the sheath at this electrode contracts. This phenomenon occurs in hydrogen plasmas due to the generation of a significant electric field reversal (i.e. one that accelerates electrons from the plasma bulk towards the electrode) when the sheath collapses, as appears in the image in the bottom row (the field reversal at the powered electrode appears in red). This field reversal occurs because the motion of electrons is hindered by collisions, and therefore a significant (reversed) electric field is necessary to accelerate the electrons to the electrode and balance the escaping ion current [40]. It only occurs close to the powered electrode since the sheath is fully expanded for most of the RF cycle, and therefore the electrons have to reach the electrode within a limited time between the sheath contraction and expansion. These electrons can then efficiently excite, or ionize, the gas. In contrast, at the grounded electrode the sheath is fully contracted for most of the RF cycle, and therefore almost no field reversal is needed to ensure current
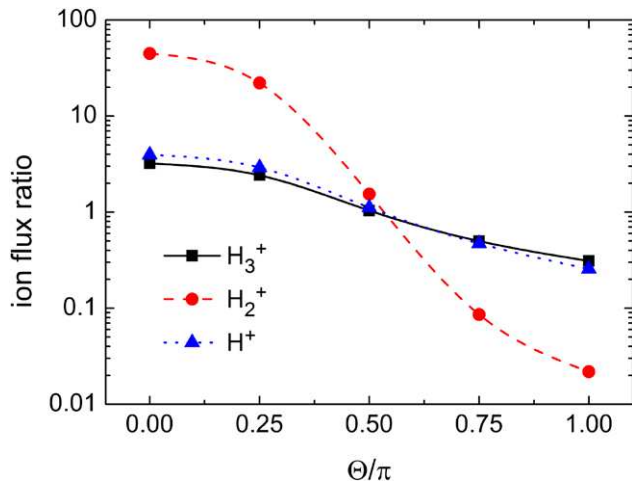
Figure 4. H_3^+ (black square), H_2^+ (red circles), and H^+ (blue triangles) ratio of the flux at the powered electrode and the flux at the grounded electrode, as a function of Θ, predicted by the PIC simulations. Lines are a guide to the eye.

balance. These results are consistent with simulation results by Mohr *et al* [30], for two-frequency driven plasmas, where such excitation due to field reversal was predicted. Following these two quasi-simultaneous excitation peaks, a final one is caused by the fast sheath expansion at the powered electrode. The amplitude of this excitation peak is larger than that occurring during sheath expansion at the grounded electrode, and is similar to that observed in argon at high pressure [5].

As previously stated, the excitation rate due to field reversal is generally overestimated by the simulations. A likely origin of this is that simulations usually underestimate the electron density [29], and therefore a larger field reversal is needed to balance the ion flux in the simulations in comparison to the experiments. This larger field reversal in the simulations would accelerate the electrons more strongly, leading to an overestimation of the excitation rate.

Further considering figure 3, one can clearly see that the excitation rate is spatially asymmetric in all cases, and that this asymmetry depends on Θ. As a consequence, the ion flux to each of the two electrodes should be different. Figure 4 shows the ion flux ratio, i.e. the ion flux at the powered electrode divided by the ion flux at the grounded electrode, for three species H_3^+ (black square), H_2^+ (red circles), and H^+ (blue triangles). Note that the *y*-axis is in log scale. It is clear that the total ion flux, which is approximately equal to the H_3^+ ion flux (since H_3^+ is by far the dominant species) is different on the two electrodes for $\Theta = 0$. The ion flux is about three times higher at the powered electrode for this waveform. The ion flux ratio decreases with Θ. It is close to unity for $\Theta = \pi/2$, and the reason for that will be studied in the next section. For $\Theta = \pi$, the ion flux is three times higher at the grounded electrode, i.e. the inverse of the $\Theta = 0$ case. This is to be expected, as a waveform corresponding to $\Theta = \pi$ is equivalent to swapping the electrodes for a waveform corresponding to $\Theta = 0$. These results show that, at this relatively high pressure (compared to [29]), it is not possible to vary the ion energy independently of the ion flux using
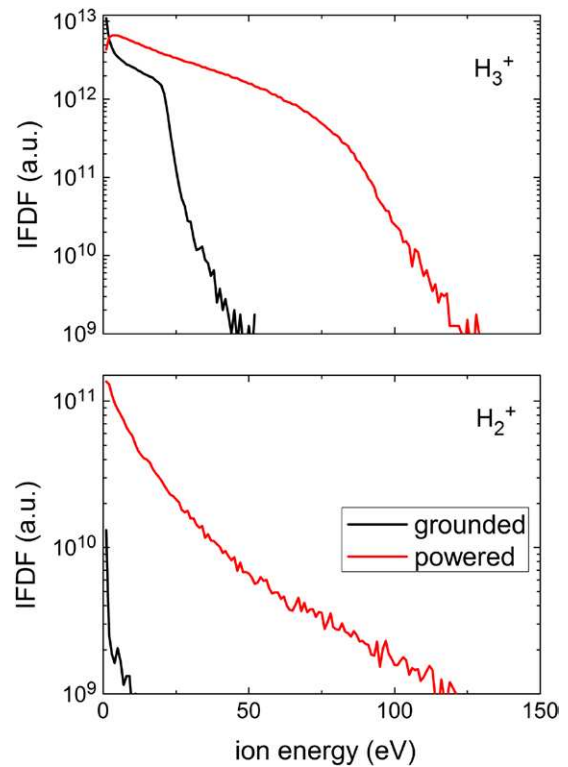

Figure 5. Ion flux distribution function (IFDF) for H_3^+ (top), and H_2^+ (bottom) for a waveform corresponding to $\Theta = 0$, determined by the PIC simulations.

the phase shift Θ, similarly to what was observed in Ar [3]. This is in contrast with the low pressure case [29], where the ion flux remains almost constant when varying Θ.

Surprisingly, whereas the flux ratio for H^+ ions is very similar to that for H_3^+, it is significantly different for H_2^+ ions. Indeed, for this species, the ion flux ratio is about 50 for $\Theta = 0$, (compared to ~3 for the other two). The trend of the ion flux ratio for H_2^+ ions with Θ is similar to the other species, but has a much larger value.

This behavior of the H_2^+ ion flux ratio can be explained in terms of its creation pathway. H_2^+ ions are mainly created within the sheath by collisions between energetic H_3^+ ions and the neutral gas. The reaction rate depends strongly on the H_3^+ energy, with an energy threshold of about 18 eV [41]. Figure 5 shows the ion flux distribution function (IFDF) for H_3^+ (top) and H_2^+ (bottom), at the powered (red line) and grounded (black line) electrodes, for a waveform corresponding to $\Theta = 0$. Note that the IFDF is shown in log scale. The unit for the IFDF is a number of counts over a certain average time in the simulations. As a consequence, the IFDF for H_3^+ and for H_2^+ can be compared with each other. Ions with high energy (up to about 120 eV) are found at the powered electrode, whereas at the grounded electrode, the ion energy does not exceed 50 eV, consistent with the strong negative DC self-bias obtained with this waveform, (observed in figure 2). In addition, very few H_3^+ ions have an energy above 25 eV at the grounded electrode.
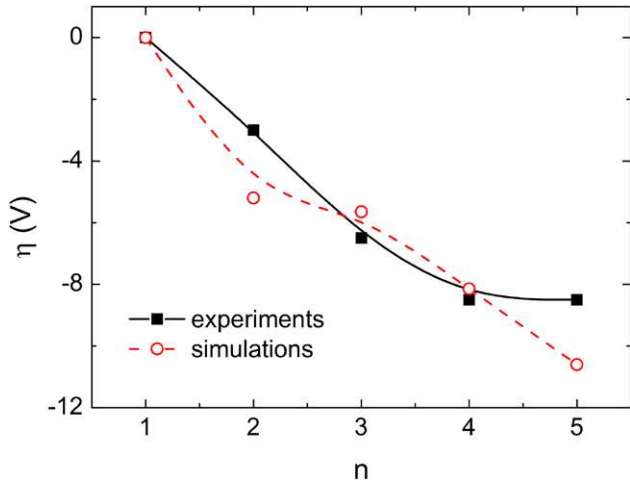
Figure 6. DC self-bias voltage η, experimentally measured (solid lines and full symbols), and obtained from PIC simulations (dashed lines and open symbols), as a function of n, for sawtooth-up waveforms. Lines are a guide to the eye.

Integrating the IFDF for ion energies above 18 eV gives an indication of the number of H_3^+ ions with energies sufficient to create H_2^+ ions via collisions with neutral H_2 molecules. The ratio of this integral at the powered electrode to that at the grounded electrode is found to be about 15. The large difference in the number of H_3^+ ions with energies above 18 eV at the two electrodes is therefore the main cause for the large ion flux ratio observed in figure 4. Furthermore, the cross section for the H_2^+ creation reaction is about one order of magnitude higher for H_3^+ ion energy of 100 eV compared to an ion energy of 20 eV, hence the very energetic ions at the powered electrode will be even more efficient in producing H_2^+ ions.

In short, due to the strong dependence of the creation rate on ion energy, controlling the H_3^+ ion energy therefore allows the H_2^+ flux ratio to be controlled. This effect was not observed at lower pressure [29].

Slope asymmetry

In the following, waveforms according to equation (4), i.e. sawtooth waveforms, are used, and the number of frequencies composing the waveform n is varied to control the slope asymmetry of the waveform, as shown in figure 1(b). The neutral gas pressure is kept constant at 900 mTorr, and the peak-to-peak voltage V_{PP} is kept at 350 V.

Figure 6 shows the DC self-bias η obtained in a H_2 discharge excited with a sawtooth-up waveform with $n = 1$–5. Both the experimental data (black solid line and squares) and the results of simulations (red dashed line and circles) are shown. Experimental data are shifted by 1 V, corresponding to the DC self-bias for the case $n = 1$, to correct for the remaining geometrical asymmetry of the reactor. As one can see, the DC self-bias remains very low for all values of n. Indeed, it is much lower than the DC self-bias that was observed in Ar for similar conditions [19].

It was previously shown [18] that in Ar plasmas the DC self-bias obtained with sawtooth waveforms is strongly correlated to the ion flux ratio through equation (1), and therefore to the spatial asymmetry of the excitation rate. The low value of the DC self-bias in hydrogen can therefore be explained by the dynamics of the electron power absorption (reflected by the excitation rate). Figure 7 shows the excitation rate extracted from optical emission of the H_α line at 656 nm (top row), and obtained from simulations (middle row) for a discharge excited with a sawtooth-up waveform with $n = 1$ to 5 (from left to right). The images are normalized to the maximum of the case $n = 5$. The bottom row displays the dynamics of the electric field outside of the sheath regions. The scale is the same for the five images of the electric field. It should be noted that for low n, and particularly for $n = 1$, the time-averaged electron density (not shown) is significantly lower than the time-averaged ion density in the inter-electrode gap, which means that no quasi-neutral bulk plasma can be defined. In these conditions (low n) it is not clear whether the Brinkmann criterion used here is fully appropriate to describe the sheath edge and therefore one should proceed with caution when considering the edges displayed in figure 7. It is nevertheless used for consistency with the results of the previous section.

There is excellent agreement in the excitation rates between the simulations and the experiments, both in the observed features and in their relative amplitude. For $n > 2$, two excitation peaks can be observed; one close to the powered electrode, immediately followed by another one close to the grounded electrode. Whereas the first excitation peak is due to the fast sheath expansion at the powered electrode, similar to the argon case [20], the second one occurs during the fast sheath contraction at the grounded electrode. This is due to the field reversal which appears at that time, as shown in the bottom row, and which accelerates the bulk electrons towards the grounded electrode. It should be mentioned that, although weaker, a field reversal also occurs at the grounded electrode when the sheath collapses. The intensity of these field reversals therefore only depends on how fast the sheath contracts. When the sheath at the powered electrode contracts rapidly, the electron thermal flux is too low to ensure current balance, and a high, reversed, electric field is necessary. In contrast, the sheath contraction at the grounded electrode is slow, and therefore a weaker reversed electric field is sufficient to ensure current balance. As one can see, this field reversal becomes stronger as n is increased, therefore balancing the increase of the excitation from sheath expansion. As a consequence of these two excitation peaks, which are of similar amplitude for the conditions studied here, negligible discharge asymmetry occurs, hence the low DC self-bias observed in figure 6.

For all species, the ratio of the ion fluxes to the two electrodes (not shown) remains close to unity for all values of n. This is because the spatial asymmetry of the excitation rate is small for sawtooth-like waveforms, as can be inferred from figure 7. Figure 8 shows the predicted IFDF at the powered (top) and grounded (bottom) electrodes, for H_3^+ (left) and H^+ (right) ions. For H_2^+ ions, the IFDF is simply an intermediate case and is therefore not shown. When n is increased,
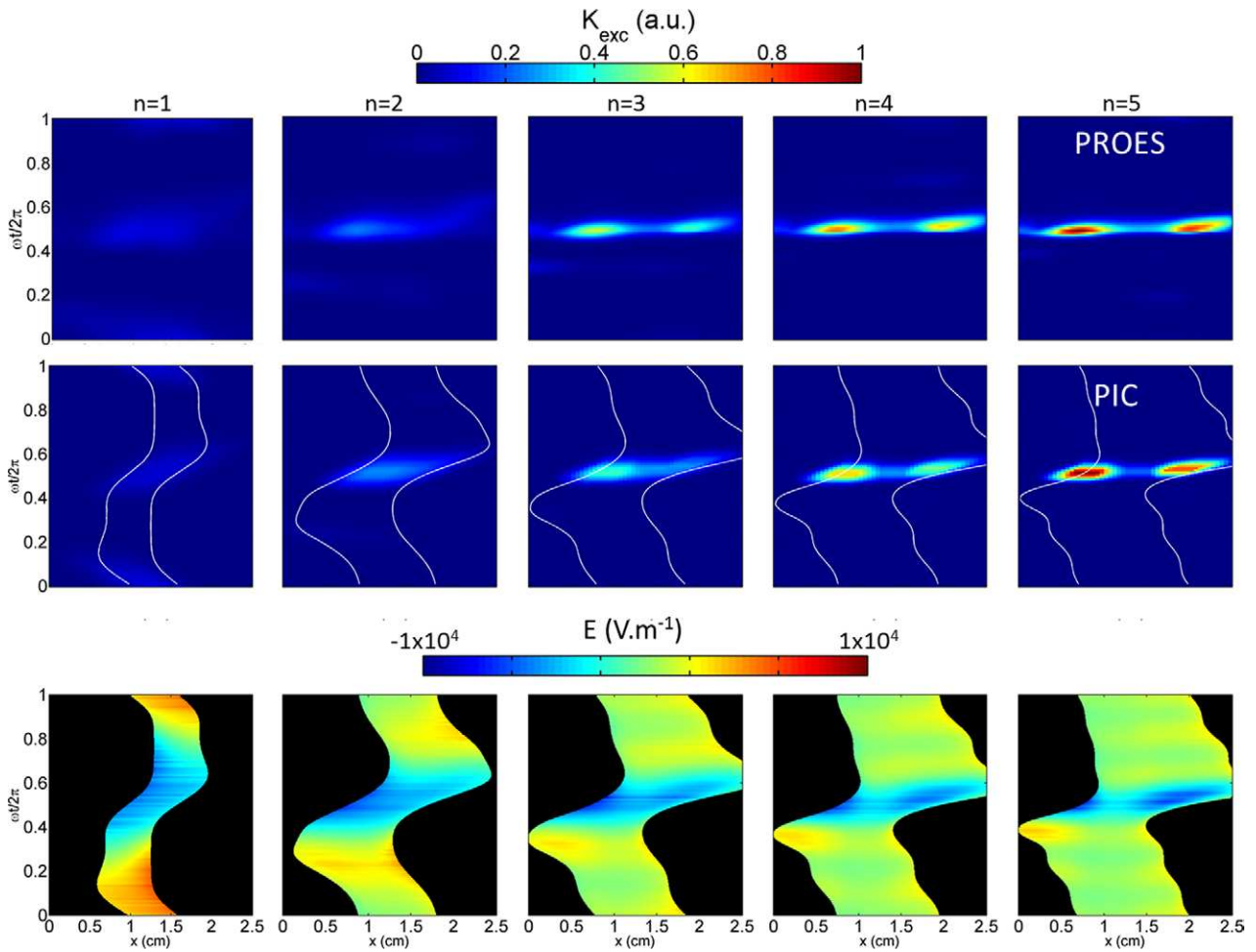
Figure 7. Excitation rate extracted from optical emission of the H_α line at 656 nm (top row), and obtained from PIC simulations (middle row), and predicted bulk electric field (bottom row) for a discharge excited with a sawtooth-up waveform with $n = 1$–5 (from left to right); the excitation rates are normalized by the maximum for the case $n = 5$.
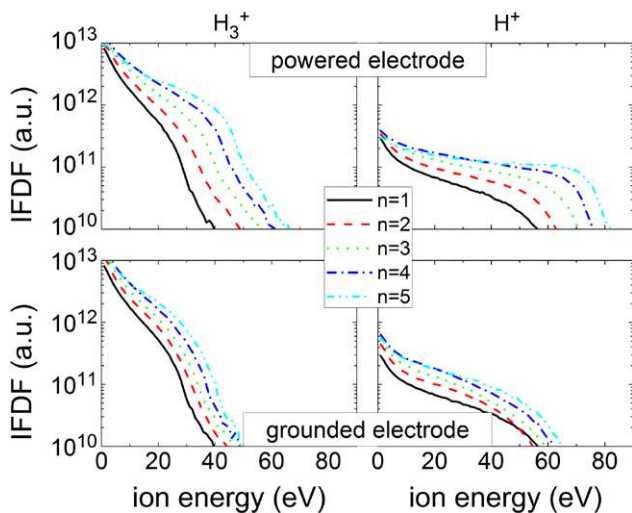

Figure 8. Ion flux distribution function (IFDF) at the powered (top) and grounded (bottom) electrode, for H_3^+ (left), and H^+ (right) ions, predicted by the PIC simulations for different values of n.

the high energy tail of the IFDF increases more significantly at the powered electrode compared to the grounded electrode for both H_3^+ and H^+. This is because, as observed in

figure 7, the excitation peak at the grounded electrode side occurs in a region which is within the sheath for most of the cycle. Therefore, ions in this region are less accelerated than those close to the powered electrode, where the excitation peak occurs farther from the electrode.

In addition, under these conditions, the ion plasma frequencies of H_3^+ and H^+ are about 2.5 MHz and 4.5 MHz, respectively, i.e. they are comparable to the fundamental frequency of 5 MHz. As a consequence, these ions are affected by the instantaneous potential to some extent, and not only the time-averaged potential. Immediately after the excitation peak, ions close to the powered electrode experience a fully extended sheath, while those close to the grounded electrode experience a fully collapsed sheath. As a consequence, the energy gain for the ions close to the powered electrode is greater than that for ions close to the grounded electrode. These two effects combine, explaining the difference in the high energy tail of the IFDFs at each electrode.

Conclusions

The impact of tailored voltage waveforms (TVWs) on parallel plate capacitively coupled hydrogen discharges was investigated, focusing on the comparatively high pressure

(~1 Torr) regime, which is often used for thin film deposition. Using amplitude asymmetric waveforms, it was found that strong field reversal occurs close to the electrode where the sheath is expanded for most of the RF cycle, i.e. where the highest ion energy is observed. As a consequence of this field reversal, higher ionization occurs close to this electrode, leading to higher ion flux. Therefore, the decoupling between ion flux and ion energy is limited under these conditions. Unexpectedly, it was found that a large ratio (~50) in the H_2^+ flux on the powered electrode compared to the grounded electrode is due to the difference in the H_3^+ energy distribution on the two electrodes. The main creation path for H_2^+ is collisions of H_3^+ ions with H_2 molecules, and the rate of this process increases strongly with H_3^+ energy, which was much higher on the powered electrode.

When the hydrogen discharge is excited with slope asymmetric waveforms, such as sawtooth waveforms, strong excitation is observed during the fast sheath expansion, as well as during the fast sheath contraction at the opposite electrode. The latter occurs due to a strong field reversal, which is needed to accelerate electrons from the plasma bulk to the electrode to balance the ion flux. As a consequence, only weak spatial asymmetry in the excitation rate is observed, and the ion flux to the two electrodes is similar.

The results of this work provide an improved understanding of the effect of TVWs on hydrogen discharges at relatively high pressure. They can be used to optimize the application of the electrical asymmetry effect in hydrogen-containing discharges used for surface modification of materials.

Acknowledgments

References

[1] Heil B G, Czarnetzki U, Brinkmann R P and Mussenbrock T 2008 On the possibility of making a geometrically symmetric RF-CCP discharge electrically asymmetric *J. Phys. D: Appl. Phys.* **41** 165202

[2] Schulze J, Schüngel E, Czarnetzki U and Donkó Z 2009 Optimization of the electrical asymmetry effect in dual-frequency capacitively coupled radio frequency discharges: experiment, simulation, and model *J. Appl. Phys.* **106** 063307

[3] Donkó Z, Schulze J, Heil B G and Czarnetzki U 2009 PIC simulations of the separate control of ion flux and energy in CCRF discharges via the electrical asymmetry effect *J. Phys. D: Appl. Phys.* **42** 025205

[4] Korolov I, Donkó Z, Czarnetzki U and Schulze J 2012 The effect of the driving frequencies on the electrical asymmetry of dual-frequency capacitively coupled plasmas *J. Phys. D: Appl. Phys.* **45** 465205

[5] Lafleur T and Booth J P 2012 Control of the ion flux and ion energy in CCP discharges using non-sinusoidal voltage waveforms *J. Phys. D: Appl. Phys.* **45** 395203

[6] Lafleur T, Delattre P A, Johnson E V and Booth J P 2012 Separate control of the ion flux and ion energy in capacitively coupled radio-frequency discharges using voltage waveform tailoring *Appl. Phys. Lett.* **101** 124104

[7] Lafleur T, Boswell R W and Booth J P 2012 Enhanced sheath heating in capacitively coupled discharges due to non-sinusoidal voltage waveforms *Appl. Phys. Lett.* **100** 194101

[8] Delattre P-A, Lafleur T, Johnson E and Booth J-P 2013 Radio-frequency capacitively coupled plasmas excited by tailored voltage waveforms: comparison of experiment and particle-in-cell simulations *J. Phys. D: Appl. Phys.* **46** 235201

[9] Coumou D J, Clark D H, Kummerer T, Hopkins M, Sullivan D and Shannon S 2014 Ion energy distribution skew control using phase-locked harmonic RF bias drive *IEEE Trans. Plasma Sci.* **42** 1880–93

[10] Zhang Y, Zafar A, Coumou D J, Shannon S C and Kushner M J 2015 Control of ion energy distributions using phase shifting in multi-frequency capacitively coupled plasmas *J. Appl. Phys.* **117** 233302

[11] Gibson A R, Greb A, Graham W G and Gans T 2015 Tailoring the nonlinear frequency coupling between odd harmonics for the optimisation of charged particle dynamics in capacitively coupled oxygen plasmas *Appl. Phys. Lett.* **106** 054102

[12] Economou D J 2013 Tailored ion energy distributions on plasma electrodes *J. Vac. Sci. Technol.* A **31** 050823

[13] O'Connell D, Gans T, Semmler E and Awakowicz P 2008 The role of the relative voltage and phase for frequency coupling in a dual-frequency capacitively coupled plasma *Appl. Phys. Lett.* **93** 081502

[14] Wang S-B and Wendt A E 2000 Control of ion energy distribution at substrates during plasma processing *J. Appl. Phys.* **88** 643–6

[15] Patterson M M, Chu H-Y and Wendt A E 2007 Arbitrary substrate voltage wave forms for manipulating energy distribution of bombarding ions during plasma processing *Plasma Sources Sci. Technol.* **16** 257–64

[16] Johnson E V, Verbeke T, Vanel J-C and Booth J-P 2010 Nanocrystalline silicon film growth morphology control through RF waveform tailoring *J. Phys. D: Appl. Phys.* **43** 412001

[17] Schulze J, Schüngel E, Donkó Z and Czarnetzki U 2011 The electrical asymmetry effect in multi-frequency capacitively coupled radio frequency discharges *Plasma Sources Sci. Technol.* **20** 015017

[18] Bruneau B, Novikova T, Lafleur T, Booth J P and Johnson E V 2014 Ion flux asymmetry in radiofrequency capacitively-coupled plasmas excited by sawtooth-like waveforms *Plasma Sources Sci. Technol.* **23** 065010

[19] Bruneau B, Novikova T, Lafleur T, Booth J P and Johnson E V 2015 Control and optimization of the slope asymmetry effect in tailored voltage waveforms for capacitively coupled plasmas *Plasma Sources Sci. Technol.* **24** 015021

[20] Bruneau B, Gans T, O'Connell D, Greb A, Johnson E V and Booth J-P 2015 Strong ionization asymmetry in a geometrically symmetric radio frequency capacitively coupled plasma induced by sawtooth voltage waveforms *Phys. Rev. Lett.* **114** 125002

[21] Bruneau B, Lafleur T, Booth J-P and Johnson E 2016 Controlling the shape of the ion energy distribution at constant ion flux and constant mean ion energy with tailored voltage waveforms *Plasma Sources Sci. Technol.* **25** 025006

[22] Johnson E V, Pouliquen S, Delattre P A and Booth J P 2011 Control of nanocrystalline silicon growth phase and deposition rate through voltage waveform tailoring during PECVD *MRS Proc.* **1339**

[23] Bruneau B, Wang J, Dornstetter J-C and Johnson E V 2014 Growth mechanisms study of microcrystalline silicon deposited by SiH$_4$/H$_2$ plasma using tailored voltage waveforms *J. Appl. Phys.* **115** 084901

[24] Hrunski D, Janssen A, Fritz T, Hegemann T, Clark C, Schreiber U and Grabosch G 2013 The influence of the electrical asymmetry effect on deposition uniformity of thin silicon film *Thin Solid Films* **532** 56–9

[25] Bruneau B, Cariou R, Dornstetter J, Lepecq M, Maurice J, Roca i Cabarrocas P and Johnson E V 2014 Ion energy threshold in low-temperature silicon epitaxy for thin-film crystalline photovoltaics *IEEE J. Photovolt.* **4** 1361–7

[26] Johnson E V, Delattre P A and Booth J P 2012 Microcrystalline silicon solar cells deposited using a plasma process excited by tailored voltage waveforms *Appl. Phys. Lett.* **100** 133504

[27] Hrunski D *et al* 2013 Deposition of microcrystalline intrinsic silicon by the electrical asymmetry effect technique *Vacuum* **87** 114–8

[28] Bruneau B, Lepecq M, Wang J, Dornstetter J, Maurice J and Johnson E V 2014 Effect of ion energy on microcrystalline silicon material and devices: a study using tailored voltage waveforms *IEEE J. Photovolt.* **4** 1354–60

[29] Diomede P, Economou D J, Lafleur T, Booth J-P and Longo S 2014 Radio-frequency capacitively coupled plasmas in hydrogen excited by tailored voltage waveforms: comparison of simulations with experiments *Plasma Sources Sci. Technol.* **23** 065049

[30] Mohr S, Schüngel E, Schulze J and Czarnetzki U 2013 Field reversals in electrically asymmetric capacitively coupled radio-frequency discharges in hydrogen *J. Phys. D: Appl. Phys.* **46** 435201

[31] Mohr S, Schungel E, Schulze J and Czarnetzki U 2014 Ion distribution functions in electrically asymmetric capacitively coupled radio-frequency discharges in hydrogen *IEEE Trans. Plasma Sci.* **42** 2376–7

[32] Bruneau B *et al* 2016 Effect of gas properties on the dynamics of the electrical slope asymmetry effect in capacitive plasmas: comparison of Ar, H$_2$ and CF$_4$, *Plasma Sources Sci. Technol.* **25** 01LT02

[33] Diomede P, Longo S, Economou D J and Capitelli M 2012 Hybrid simulation of a dc-enhanced radio-frequency capacitive discharge in hydrogen *J. Phys. D: Appl. Phys.* **45** 175204

[34] Hockney R W and Eastwood J W 1988 *Computer Simulation Using Particles* (Boca Raton, FL: CRC Press)

[35] Longo S 2006 Monte Carlo simulation of charged species kinetics in weakly ionized gases *Plasma Sources Sci. Technol.* **15** S181–8

[36] Gans T, O'Connell D, Schulze-von der Gathen V and Waskoenig J 2010 The challenge of revealing and tailoring the dynamics of radio-frequency plasmas *Plasma Sources Sci. Technol.* **19** 034010

[37] Brinkmann R P 2007 Beyond the step model: approximate expressions for the field in the plasma boundary sheath *J. Appl. Phys.* **102** 093303

[38] Godyak V A 1972 Statistical heating of electrons at an oscillating plasma boundary *Sov. Phys.—Tech. Phys.* **16** 1073–6

[39] Lieberman M A and Lichtenberg A J 2005 *Principles of Plasma Discharges and Materials Processing* (New York: Wiley)

[40] Czarnetzki U, Luggenhölscher D and Döbele H F 1999 Space and time resolved electric field measurements in helium and hydrogen RF-discharges *Plasma Sources Sci. Technol.* **8** 230

[41] Phelps A V 1990 Cross sections and swarm coefficients for H$^+$, H^{2+}, H^{3+}, H, H$_2$, and H$^-$ in H$_2$ for energies from 0.1 eV–10 keV *J. Phys. Chem. Ref. Data* **19** 653–75